

Shamloo, H., and Grunder, A., 2023, Magma mingling and ascent in the minutes to hours before an explosive eruption as recorded by banded pumice: *Geology*, <https://doi.org/10.1130/G51318.1>

Supplemental Material

Additional figures with discussion of analytical and modeling methods (File S1: Figs. S1–S6), data collected (File S2: Tables S1–S4), and Python script (File S3).

GSA Data Repository

Shamloo and Grunder: Magma mingling and ascent in the minutes to hours before an explosive eruption as recorded by banded pumice.

SUPPLEMENTARY INFORMATION

1. Electron Microprobe Analysis and Heating Experiment

All samples were collected from the Rattlesnake Tuff (RST) in Central Oregon at Delintment Lake (see Streck and Grunder, 1995). Chemical gradients (i.e., a transect of points) were measured across visible band boundaries using wave dispersive spectroscopy (WDS) on a Cameca SX-100 Electron Microprobe at Oregon State University. Major elements plus Cl and Ba were measured in 27 total transects from 7 individual samples (as carbon-coated thin sections) using a 10 μm beam diameter, 15 kV voltage, and 10 nA beam current. The reproducibility of standards was typically better than 1 wt% relative for concentrations > 10 wt%, and 2–10 wt% relative for concentrations of 0.1–1 wt%. Primary and secondary standards used included Old Crow Rhyolite UA1099 and RHYO VG-568.

Analytical challenges involved placing a 10 μm beam diameter as a line of evenly spaced points on glass while avoiding vesicles. Due to the vesiculation of the samples, individual point locations were manually chosen to guarantee analysis on glass and not epoxy in a vesicle. Therefore, the resulting line of points are offset in both the X and Y direction (i.e., unevenly spaced and offset from a line). Points were projected back onto a single line using simple geometry to correct for offset in the Y-direction but remained unevenly spaced in the X-direction, but in most cases yielded satisfactory profiles. The spacing between points ranged anywhere from 10 to 100s μm .

All totals less than 94% (unnormalized) were eliminated, based on approximate water estimates via secular hydration of RST glass. As much as 6 wt% H_2O was added to pumice samples post-deposition determined via heating experiments of RST glass shards from fall deposits (Grunder et al., 2005). Additionally, we conducted a simple heating experiment in this study by taking thick sections of banded pumice (free of epoxy) and placed it in a platinum crucible in a muffle furnace in air. Two experiments were conducted: one at 550°C for 17 d, and one at 900°C for 4 d. The thick sections were weighed before and after heating. The weight loss for the low temperature experiment was 0.046 g, and 0.049 g for the high temperature experiment. If assuming the weight lost from the pumice samples was entirely water loss, these indicate ~4 wt% H_2O released. Together, these estimates imply that the RST was hydrated post-deposition anywhere from 4–6 wt% H_2O , which informed which electron microprobe totals were acceptable or not.

2. Diffusion Chronometry & Assessment of Uncertainty

Modeling the time of diffusion assumes an initial condition of a step-function at the boundary (in this case, between two juxtaposed magmas), and employs an analytical solution to Fick's Second Law, involving one-dimensional diffusion in an infinite medium with an abrupt change in composition when the diffusion distance is small (Costa and Morgan, 2010; Costa et al., 2020):

$$C = C_0 + \frac{C_1 - C_0}{2} \left[\operatorname{erfc} \frac{x}{2\sqrt{Dt}} \right] \quad (1)$$

where C is the normalized concentration, C_0 and C_1 are the initial amounts of the element on each side of the interface at time zero, D is the diffusivity ($\text{m}^2 \text{s}^{-1}$), t is the diffusion time, and x is distance on the concentration profile. Diffusivities were calculated using Equation 2:

$$D = D_0 e^{\left(\frac{-E}{RT}\right)} \quad (2)$$

using the Arrhenius parameters (E_A and D_0) experimentally determined for Si and Ba diffusion in rhyolite. Values for Si diffusion in a wet rhyolite (3 wt% H_2O) was used from Baker (1991), and values for Ba diffusion in rhyolite was used from Magaritz and Hofmann (1978). We used a Monte Carlo least-square minimization procedure implemented in Python to find the complementary error function that best fit each observed element profile by iteratively varying the concentration of each plateau incorporating the error in concentration, the center of the diffusion profile to account for the uncertainty in distance (i.e., uneven spacing of measurements), and diffusion length scale (\sqrt{Dt})—considering the uncertainty in Arrhenius parameters D_0 and E_A following the methods of Brugman et al. (2022). Given the range of variables explored in the models, we report a best-fit timescale as a time *interval* which includes a distribution of times associated with a range of temperatures, diffusion coefficients, and spacing of concentration points. See further discussion of uncertainty below. Note Arrhenius parameters for Ba and Si diffusion in rhyolite were determined at different pressures (1 atm for Ba; 1 GPa for Si), however it has been suggested that pressure has negligible effect on diffusion compared to temperature (Zhang, 2010). Also see File S3 (.ipynb file) to view the script written in Jupyter Notebook, Python version 3.7.15.

2.1 Uncertainty 1: The Role of Water on Diffusion

The pre-eruptive water concentration of the RST was likely between 2–4 wt% H_2O and no higher than 5.0–5.5 wt% H_2O (Swenton and Streck, 2022; Grunder and Grunder, 1997). Additionally, barometry indicates magma storage of the RST was generally at a little less than 200 MPa. Diffusivity values for Si in rhyolite exist at variable water contents including dry rhyolite (Baker, 1990; 1992) and rhyolite with 3 and 6 wt% H_2O (Baker, 1991). Given our water estimates for the RST and the unlikelihood that the RST is a dry rhyolite, we favor the diffusivity at 3 wt% H_2O from Baker (1991). Modeling diffusion times using the diffusivity of Si in rhyolite with 3 wt% H_2O yields Si and Ba timescales in agreement of each other. When modeling with the diffusivity of 6 wt% H_2O , the Ba and Si diffusion timescales disagree by an order of magnitude or more. Additionally, the widths of Ba and Si profiles for a given transect are similar; an observation that may indicate that the profile of each chemical species is recording similar amounts of diffusive relaxation, which further supports the use of the diffusion coefficient at 3 wt% H_2O .

Related to water, there is also the unknown of how much water is lost from the magma in the conduit as it experiences ascent and mingling. Generally, the presence of water in magma can speed up the rate of diffusion (e.g., Baker, 1991). Therefore, water loss would subsequently lead to slower diffusion rates, causing less diffusive relaxation, which would lead to resulting timescales representing minima.

2.2 Uncertainty 2: The Challenges with Glass Analyses (Vesicles and Microlites)

As briefly discussed in the main text, the timing of vesiculation relative to the timing of diffusion is in question. If vesiculation, or formation of bubbles, occurred pre-diffusion, then the diffusion path length would be representative of the true diffusion distance yielding the actual diffusion time, or at least a minimum timescale considering the recorded time lost when temperatures drop low enough that significant diffusive relaxation is unresolvable on the probe. If vesiculation occurred post-diffusion, then the apparent diffusive path (or distance) measured on the probe would be lengthened. Consequently, this would overestimate the total diffusion distance and therefore the total timing of diffusion. This would in turn yield maximum timescales. The likely scenario is that diffusion and vesiculation occur simultaneously given the temperature, pressure, and water content of the RST magma. Hence, while the diffusion path is being lengthened from vesiculation, diffusion is occurring. Therefore, we consider our calculated timescales of magma mingling and ascent to represent maxima.

To further test the effect of vesicles on the resulting diffusion time, a simple test was performed. Multiple transects were measured on the same band boundary with variable degrees of vesiculation. The resulting timescales are within error of each other, which indicates that either the differences in time are lost in the spatial resolution of our measurements, or the differences in timescales are enveloped in the error associated with best-fit time intervals from our modeling approach.

Lastly, the presence of microlites would likely affect the resulting chemical compositions measured via microprobe. To investigate the presence of microlites, we performed a high-resolution BSE image of a full thin section (Fig. S4). We find there are indeed microlites (likely Fe-Ti oxides due to bright greyscale in BSE, but not confirmed) present but in relatively low volume and generally in the Fe-rich rhyolite groups (i.e., rhyolites E and D). This may contribute to scatter present in rhyolite group classification (Fig. 1 main text), especially for the Fe-rich rhyolite groups, however other elemental discriminants were used to assign rhyolite groups. Additionally, it does not affect the overall Si and Ba diffusion profile shapes which are essential to diffusion modeling, therefore we do not consider the effect of microlites any further.

2.3 Addressing Uncertainty 3: The Temperature of Diffusion

Determining the exact temperature of diffusion appropriate for each diffusion profile measured is difficult to determine. Instead, the modeling approach used for this study explores a temperature range which accounts for the variable temperatures for each rhyolite group, as well as the error in the thermometry method used (Grunder and Streck, 1997; Swenton and Streck, 2022). For example, when measuring a transect across a boundary between rhyolite A and E, a wide temperature range of 760–970°C was used to reflect the lowest and highest possible temperature calculated by thermometry for each of these rhyolite groups (Swenton and Streck, 2022). Therefore, temperature is a fit variable in our model, and the best-fit profile is associated with a best-fit temperature which is reported in Table S2. Note, temperatures in the conduit are likely cooler than magma storage temperatures, which were used for modeling. However, resolvable diffusion (i.e., ≥ 10 microns, same as the spatial resolution of electron probe analysis) would not occur if the temperature was below 700°C based on a simple calculation using the square root of Dt . Therefore, we assume that most if not all of diffusion

happens at high temperature similar to storage temperatures, and that diffusion is relatively insignificant once the pumice is emplaced. Also note we use only nonwelded samples, with emplacement temperatures below 600 °C, so there is little to no concern about post-depositional diffusion (Grunder et al., 2005).

Another uncertainty related to temperature, is extracting diffusion coefficients from experimentally determined Arrhenius parameters at 1100–1400°C down to RST temperatures which are ~250°C lower. There can be complications with this approach, so at the minimum we considered a range of E_A and D_0 values reported from the respective experimental paper to be included in the calculations of diffusivity values used for modeling. It should also be noted another source of error is that our modeling approach does not include the covariance of E_A and D_0 , which has been shown to artificially produce a large range of possible diffusion coefficients (Brugman et al., 2022). This may suggest that our time intervals are over-estimated, and our modeling can be improved upon to get a higher resolution of time.

2.4 Concluding Remarks on Addressing Uncertainties

We conclude the two parameters that provide the largest uncertainty on diffusion timescales are water and temperature. Therefore, we performed a simple test to determine which parameter has the largest control on the resulting timescale in order to improve upon this method. When calculating the diffusion coefficient for Si at constant temperature but with the Arrhenius parameters for 3 and 6 wt% H₂O, the resulting diffusion coefficients are 0.2 log units different. In contrast, when calculating the diffusion coefficient for Si at two different temperatures 50°C apart, the resulting diffusion coefficient is an order of magnitude different. Therefore, temperature is far more influential on the resulting diffusion coefficient and therefore timescale than water. Because we are using magma storage temperatures that are likely higher than conduit temperatures, we conclude that our timescale intervals represent the upper end or maximum possible timescales associated with mingling and eruption.

The proposed approach to applying diffusion chronometry to vesiculated material that has experienced mingling upon ascent poses many challenges and uncertainties to reconcile. While we do our best to accommodate uncertainty in our modeling, we acknowledge the limitations of this approach and welcome future workers to improve on this study. We conclude that this study's diffusion time estimates represent maxima, and further work is required to improve the precision on time estimates.

3. VESIcal and Viscosity Calculations

Viscosity calculations were performed for each rhyolite composition recorded in RST banded pumice. First, H₂O and CO₂ contents for each electron microprobe rhyolite analysis were determined using *VESIcal* via *JupyterLab* using the ENKI portal (Wieser et al., 2022) utilizing the model of Ghiorso and Gualda (2015). *VESIcal* was run assuming a pressure of 1 kbar and a X_{fluid} value of 0.9, where X_{fluid} represents equilibrium with H₂O ($X_{fluid} = 1$) and CO₂ ($X_{fluid} = 0$). A relatively high X_{fluid} value was run due to the typical limited availability of CO₂ in a rhyolite. Resulting volatile contents for RST rhyolites was around ~3.8 wt% H₂O and 0.008 wt% CO₂ and are summarized in Table S4 in Supplemental Material File 2.

Once H₂O and CO₂ values were determined for each rhyolite analysis, viscosity calculations were performed after Giordano et al. (2008) model for volatile-bearing magmas.

Due to the crystal content being very low for the RST (<1 vol.%), crystallinity was not considered in viscosity calculations. Variable temperatures were assumed for each rhyolite group based on past thermometry that indicates a thermally and density stratified magma chamber (Streck and Grunder, 1997; Table 3 in Swenton and Streck, 2022), where rhyolite A was run at 805°C, rhyolite B at 826°C, rhyolite C at 877°C, rhyolite D at 880°C, and rhyolite E at 895°C. Resulting viscosity values are distinct for each rhyolite group and range from $10^{4.6}$ to $10^{5.8}$ Pa s (Table S4). A standard error of 5% is determined for each viscosity calculation based on Giordano et. al. (2008).

Another factor that can affect viscosity but isn't represented in the viscosity calculations, is the shape of the bubbles present (e.g., Marsh, 1981). Bubbles will either increase or decrease magma viscosity based on their capillary number, or amount of shearing, where highly deformed bubbles will decrease magma viscosity and undeformed bubbles will increase viscosity (e.g., Takeuchi, 2011). When observing the RST pumice samples, there is evidence of minor amounts of shearing that is preferentially oriented parallel to the banding itself, suggesting some shearing occurred after mingling (Fig. S4). If the bubbles in the conduit were less deformed upon the onset of eruption, bubbles would increase the viscosity of rhyolite A.

SUPPLEMENTARY FIGURES

Figure S1. Banded pumice samples from the Rattlesnake Tuff investigated in this study. Note each band is a high-silica rhyolite where the differences in color represent variable amounts of Fe. Darker bands have a higher concentration of Fe, and lighter bands have a lower concentration of Fe.

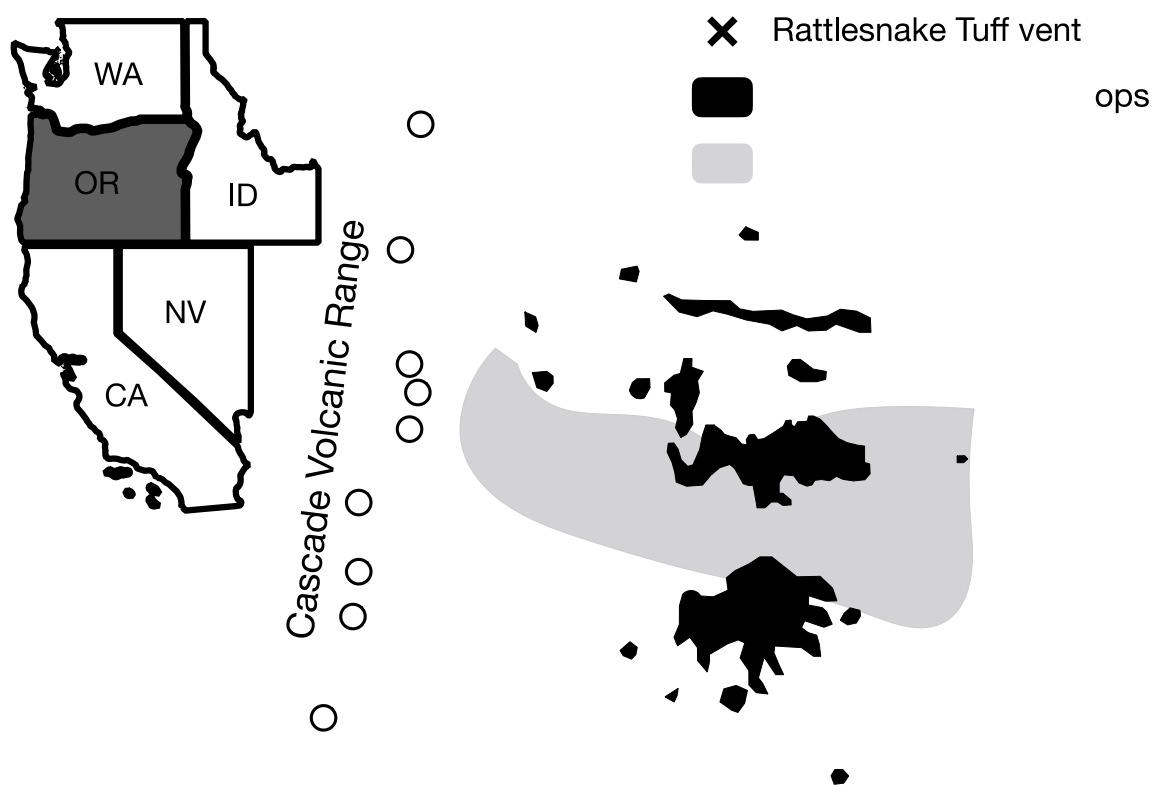


Figure S2. Map of Oregon in the United States after Streck and Grunder (2008). Black regions indicate Rattlesnake Tuff outcrops, and the “X” indicates the inferred vent/source. The gray shaded area marks the High Lava Plains of southeastern Oregon. White circles mark individual volcanoes part of the Cascade Volcanic Range.

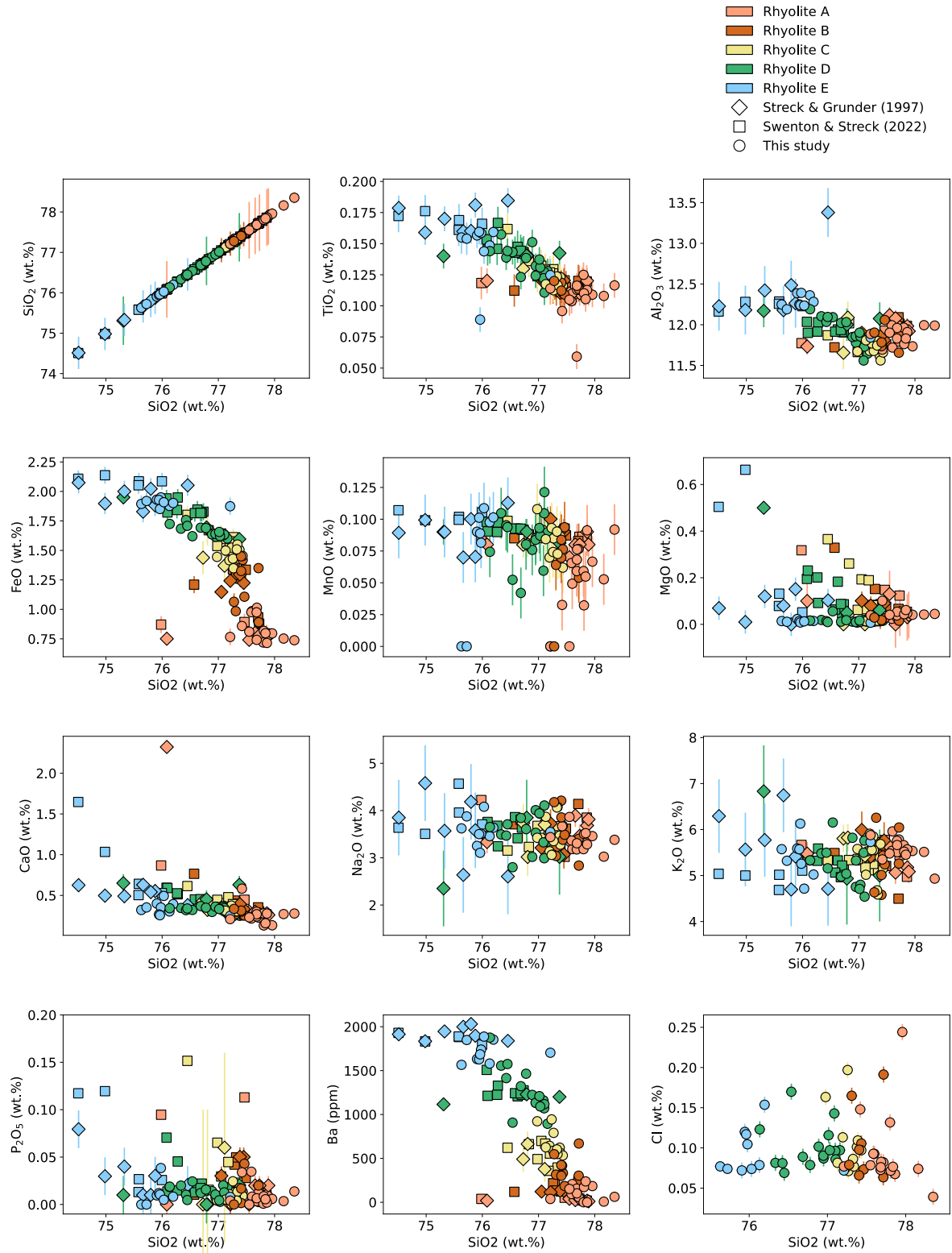


Figure S3. Major element variation diagrams collected from the electron microprobe of distinct rhyolite groups within the Rattlesnake Tuff banded pumice. Streck and Grunder (1997) data are shown by diamonds and Swenton and Streck (2022) data are shown by squares. Data is color coded based on the respective rhyolite group characterized by Streck and Grunder (1997) and Swenton and Streck (2022). This characterization was used to group the data from this study, shown by circles. All data is normalized. Data reported as 0 are measurements below detection limit.

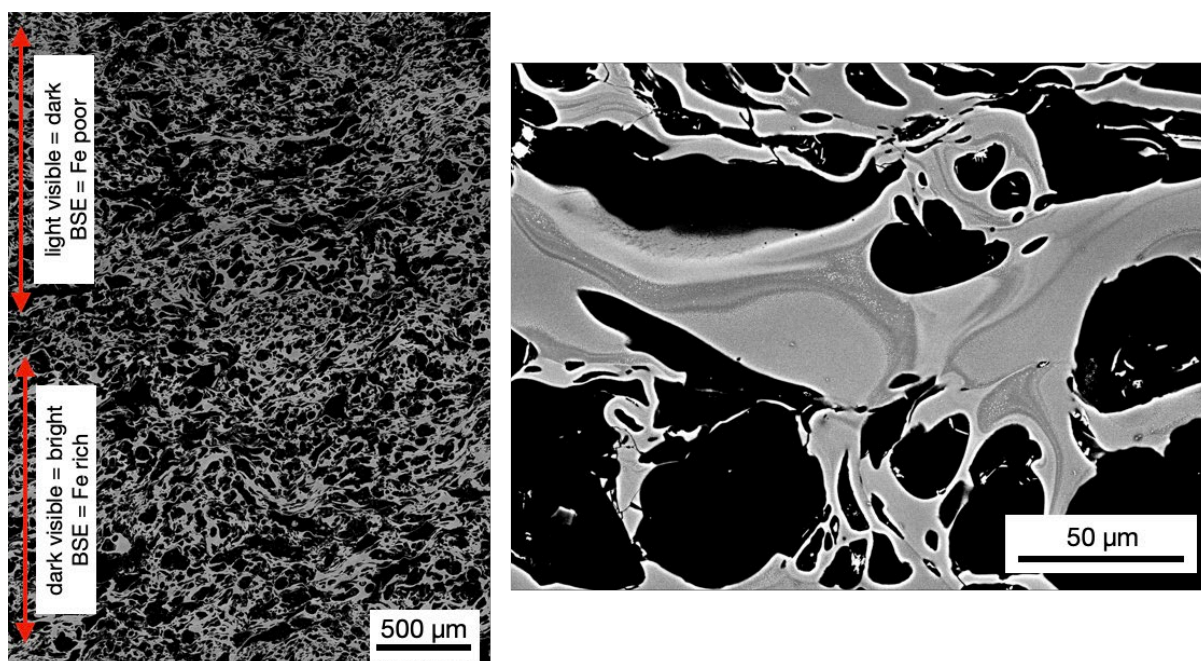
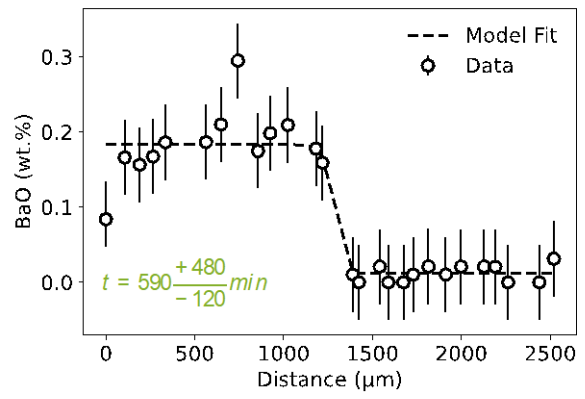
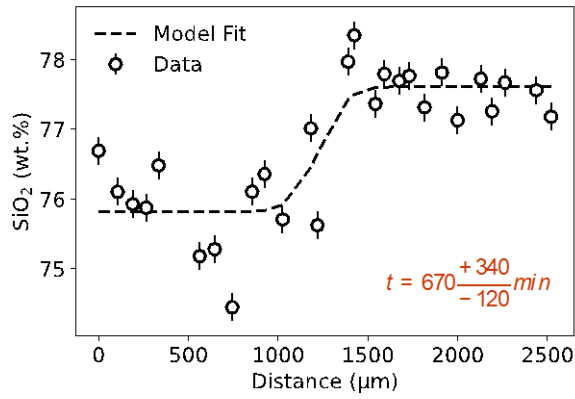
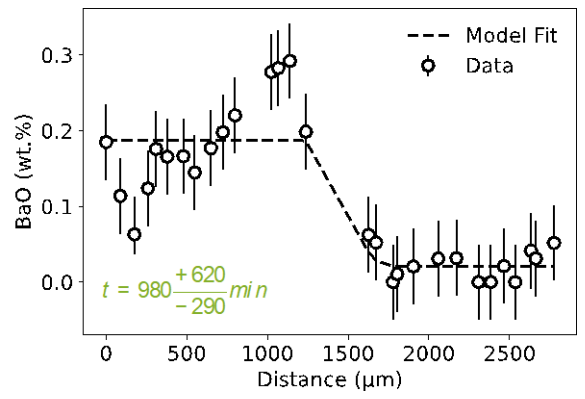
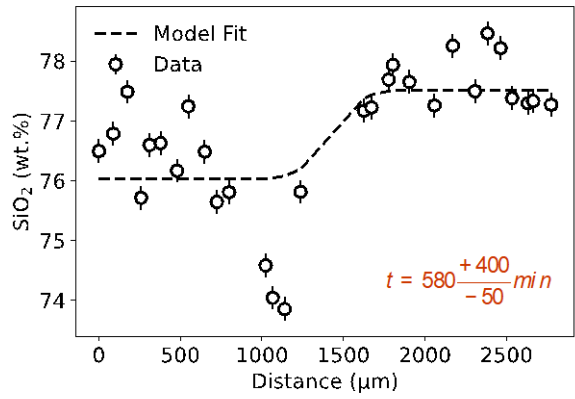


Figure S4. Backscattered electron (BSE) images of the Rattlesnake Tuff pumice covering an entire thin section (left) and a zoomed in portion (right). The BSE image shows a sharp boundary between rhyolite banding within this sample, where dark grey BSE areas (or light color in visible light) represent Fe-poor glass and light gray BSE areas represents Fe-rich glass (or dark color in visible light). Vesicularity was determined at ~70% using ImageJ software (Schneider et al., 2012). Note the fine detail of mingling as well as presence of microlites (small white specks—likely Fe-Ti oxides but not confirmed).

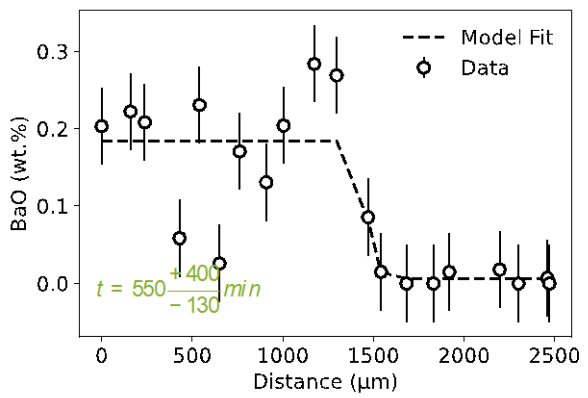
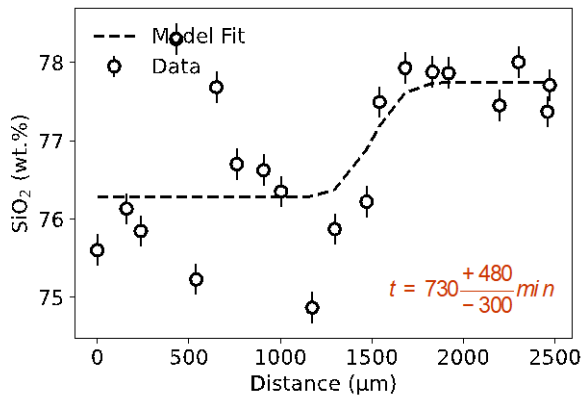
P1-A trans1 (AE)



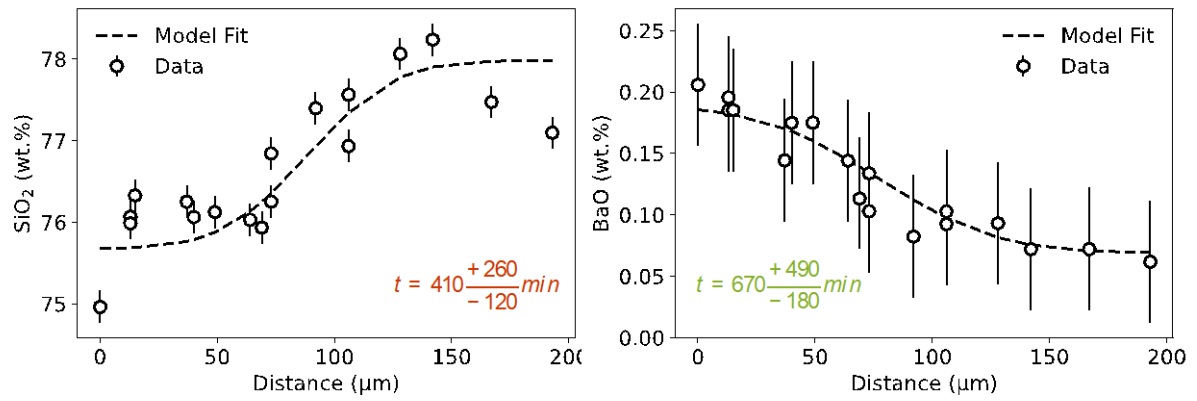
P1-A trans2 (AE)



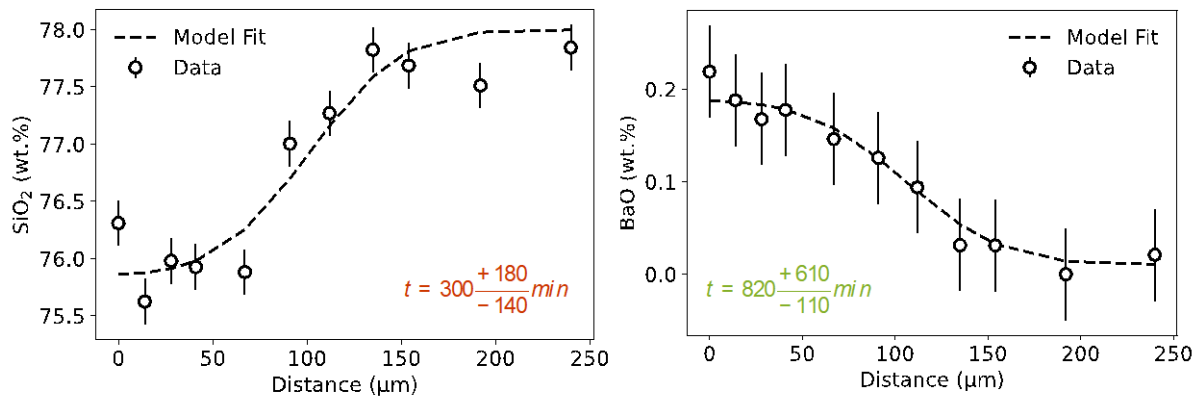
P1-A Trans6 (AE)



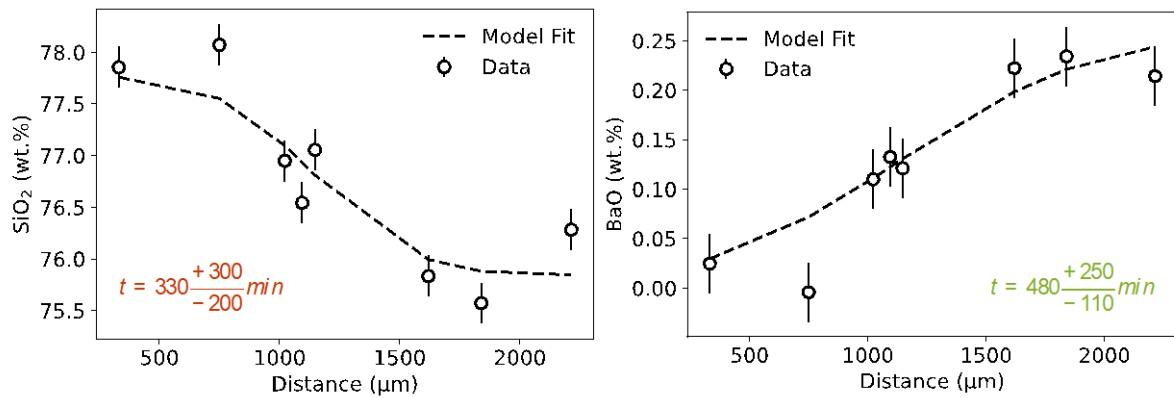
P1-A Area1 (AE)



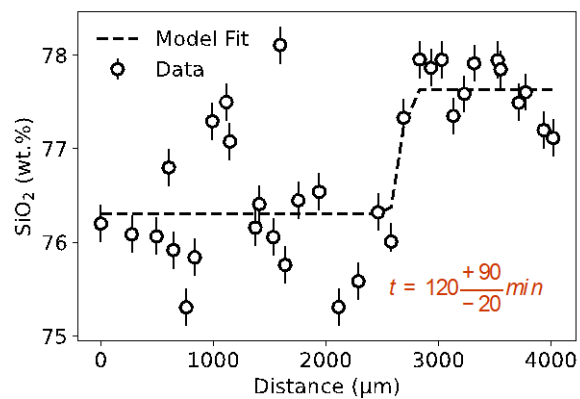
P1-A Area3 (AE)



120E-Trans3 (AD)

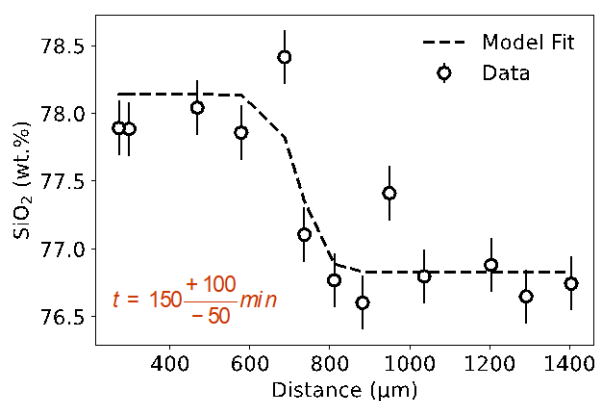


P1-A Trans7 (AD)



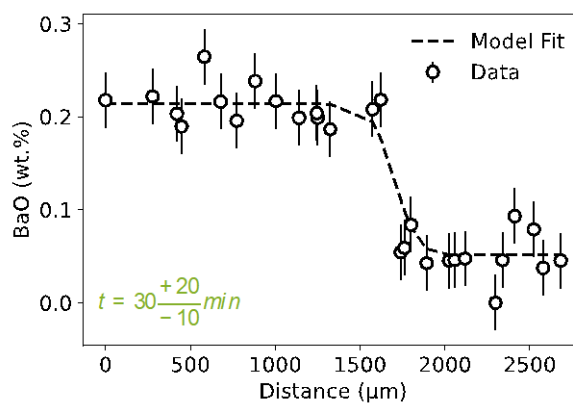
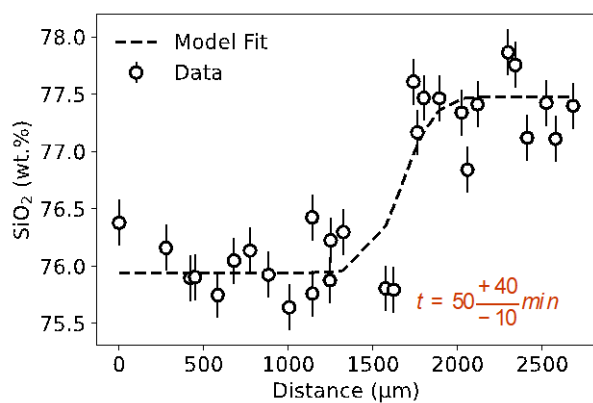
Unable to fit Ba profile

120E-Trans4.2 (AD)

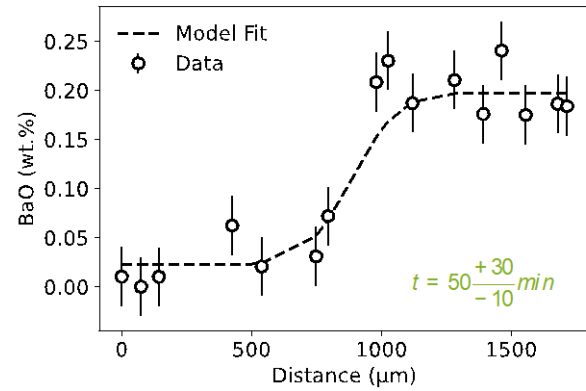
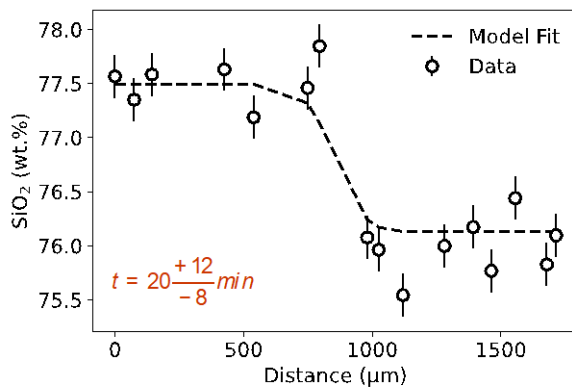


Unable to fit Ba profile

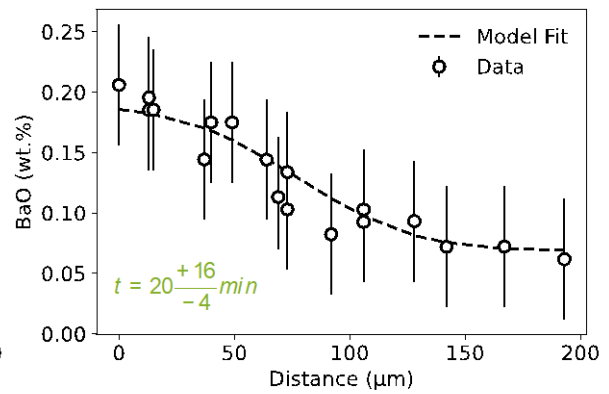
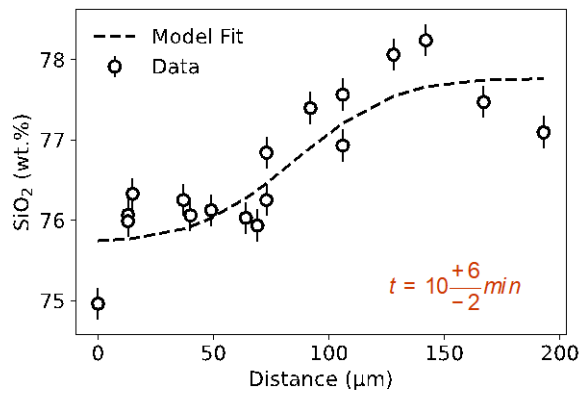
122E-Trans5 (BE)



P1-A trans3 (BE)

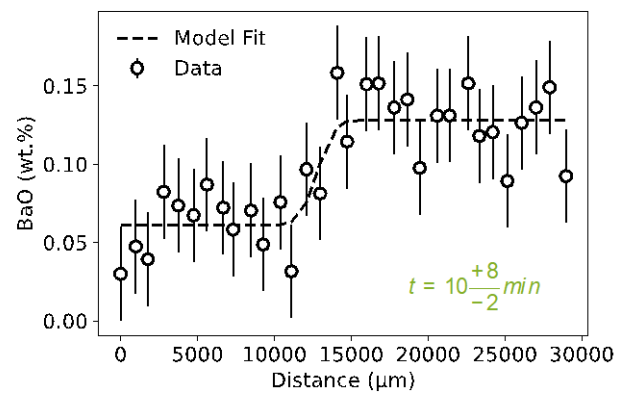


P1-A Area2 (BE)



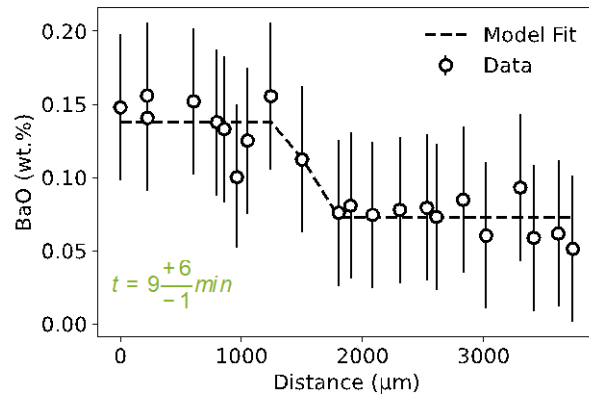
P3-Trans3 (CD)

Unable to fit Si profile



P3-Trans4 (CD)

Unable to fit Si profile



P3-Trans5 (CD)

Unable to fit Si profile

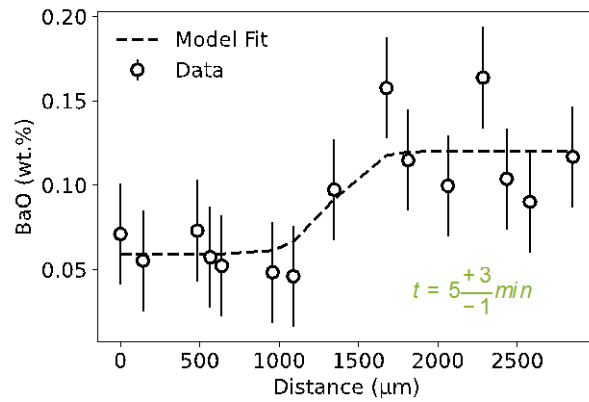


Figure S5. Chemical gradients (Si in the left column; Ba in the right column) and fitted modeled diffusion profiles (dashed line) for each transect collected on the electron microprobe. Note the time interval reported for each fit in the lower portion of the figure. Both Ba and Si were measured, but there are a few scenarios where one profile was unable to be fit by the analytical solution to the diffusion equation.

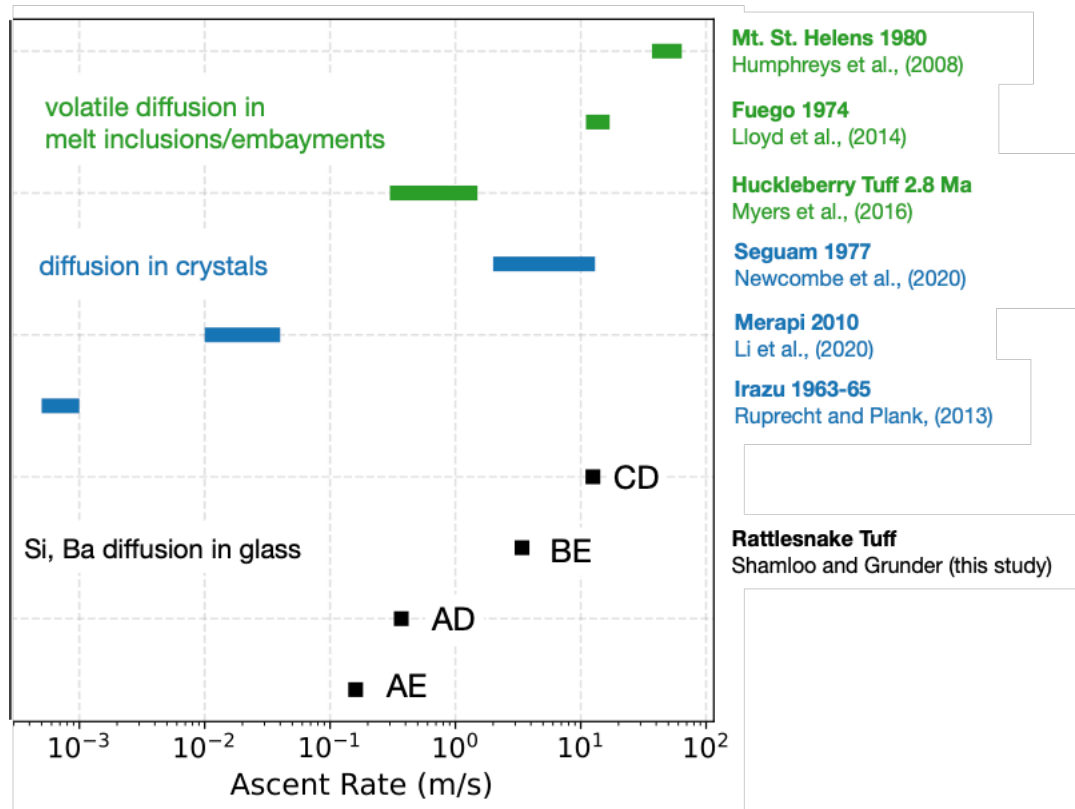


Figure S6. Examples of ascent rates for other explosive eruptions published in the literature. The top three ascent rates were determined from volatile diffusion in melt inclusions or embayments (Humphreys et al., 2008; Lloyd et al., 2014; Myers et al., 2016), the middle three were determined from diffusion in crystals (Newcombe et al., 2020; Li et al., 2020; Ruprecht and Plank, 2013), and the bottom are the ascent rates determined from this study using diffusion in glass across mingled rhyolite boundaries in banded pumice.

REFERENCES CITED IN SUPPLEMENTARY MATERIAL FILE 1

- Baker, D.R., 1990, Chemical interdiffusion of dacite and rhyolite: anhydrous measurements at 1 atm and 10 kbar, application of transition state theory, and diffusion in zoned magma chambers. *Contributions to Mineralogy and Petrology*, 104(4), 407-423.
- Baker, D.R., 1991, Interdiffusion of hydrous dacitic and rhyolitic melts and the efficacy of rhyolite contamination of dacitic enclaves. *Contributions to Mineralogy and Petrology*, 106(4), 462-473.
- Baker, D.R., 1992, Estimation of diffusion coefficients during interdiffusion of geologic melts: application of transition state theory. *Chemical Geology*, 98(1-2), 11-21.
- Blake, S., 1981, Volcanism and the dynamics of open magma chambers. *Nature*, v. 289, p. 783-785.
- Brugman, K., Till, C. B., and Bose, M., 2022, Common assumptions and methods yield overestimated diffusive timescales, as exemplified in a Yellowstone post-caldera lava. *Contributions to Mineralogy and Petrology*, v. 177(6), p. 63.
- Costa, F., and Morgan, D., 2010, Time constraints from chemical equilibration in magmatic crystals. *Timescales of magmatic processes: from core to atmosphere*, p. 125-159.
- Costa, F., Shea, T., and Ubide, T., 2020, Diffusion chronometry and the timescales of magmatic processes. *Nature Reviews Earth & Environment*, v. 1(4), p. 201-214.
- Ghiorso, M., and Gualda, G., 2015, An H₂O-CO₂ mixed fluid saturation model compatible with rhyolite-MELTS, *Contributions to Mineralogy and Petrology*, v. 169, p. 1–30.
- Giordano, D., Russell, J. K., & Dingwell, D. B., 2008, Viscosity of magmatic liquids: a model. *Earth and Planetary Science Letters*, v. 271(1-4), p. 123-134.
- Grunder, A.L., Laporte, D., and Druitt, T.H., 2005, Experimental and textural investigation of welding: effects of compaction, sintering, and vapor-phase crystallization in the rhyolitic Rattlesnake Tuff. *Journal of volcanology and geothermal research*, v. 142(1-2), p. 89-104.
- Humphreys, M. C., Menand, T., Blundy, J. D., and Klimm, K., 2008, Magma ascent rates in explosive eruptions: Constraints from H₂O diffusion in melt inclusions. *Earth and Planetary Science Letters*, 270(1-2), 25-40.
- Li, W., Costa, F., and Nagashima, K., 2021, Apatite crystals reveal melt volatile budgets and magma storage depths at Merapi volcano, Indonesia. *Journal of Petrology*, 62(4), egaal00.
- Lloyd, A. S., Ruprecht, P., Hauri, E. H., Rose, W., Gonnermann, H. M., and Plank, T., 2014, NanoSIMS results from olivine-hosted melt embayments: magma ascent rate during explosive basaltic eruptions. *Journal of Volcanology and Geothermal Research*, 283, 1-18.

- Magaritz, M., and Hofmann, A. W., 1978, Diffusion of Sr, Ba and Na in obsidian. *Geochimica et Cosmochimica Acta*, 42(6), 595-605.
- Marsh, B. D., 1981, On the crystallinity, probability of occurrence, and rheology of lava and magma. *Contributions to Mineralogy and Petrology*, 78, 85-98.
- Myers, M. L., Wallace, P. J., Wilson, C. J., Morter, B. K., and Swallow, E. J., 2016, Prolonged ascent and episodic venting of discrete magma batches at the onset of the Huckleberry Ridge supereruption, Yellowstone. *Earth and Planetary Science Letters*, 451, 285-297.
- Newcombe, M. E., Plank, T., Barth, A., Asimow, P. D., and Hauri, E., 2020, Water-in-olivine magma ascent chronometry: Every crystal is a clock. *Journal of Volcanology and Geothermal Research*, 398, 106872.
- Ruprecht, P., and Plank, T., 2013, Feeding andesitic eruptions with a high-speed connection from the mantle. *Nature*, 500(7460), 68-72.
- Schneider, C.A., Rasband, W.S., Eliceiri, K.W., 2012, NIH Image to ImageJ: 25 years of image analysis. *Nature Methods* v. 9, p. 671-675, <https://imagej.nih.gov/ij/>
- Streck, M.J., and Gruner, A.L., 1995, Crystallization and welding variations in a widespread ignimbrite sheet; the Rattlesnake Tuff, eastern Oregon, USA. *Bulletin of Volcanology*, v. 57, p. 151-169.
- Streck, M., and Gruner, A.L., 1997, Compositional gradients and gaps in high-silica rhyolites of the Rattlesnake Tuff, Oregon. *Journal of Petrology*, v. 38, p. 133-163.
- Streck, M.J., and Gruner, A.L., 2008, Phenocryst-poor rhyolites of bimodal, tholeiitic provinces: the Rattlesnake Tuff and implications for mush extraction models. *Bulletin of Volcanology*, v. 70, p. 385-401.
- Swenton, V.M., and Streck, M.J., 2022, Pre-Eruptive Magma Configurations and Petrogenetic Relationships of the Rattlesnake Tuff, Oregon—Insights From Spectacularly Banded High-Silica Rhyolite Pumices. *Frontiers in Earth Science*, v. 10, p. 841279.
- Takeuchi, S., 2011, Preeruptive magma viscosity: An important measure of magma eruptibility. *Journal of Geophysical Research: Solid Earth*, v. 116.
- Wieser, P.E., Iacovino, K., Matthews, S., Moore, G., and Allison, C.M., 2022, VESIcal: 2. A Critical Approach to Volatile Solubility Modeling Using an Open-Source Python3 Engine. *Earth and Space Science*, v. 9(2), e2021EA001932.
- Youxue Zhang, 2010, Diffusion in Minerals and Melts: Theoretical Background. *Reviews in Mineralogy and Geochemistry*; 72 (1): 5–59. doi: <https://doi.org/10.2138/rmg.2010.72.2>